Int J Earth Sci (Geol Rundsch) (2010) 99:427–441
DOI 10.1007/s00531-008-0393-1

ORIGINAL PAPER

Interaction between tectonic and erosion processes on the morphogenesis of an Alpine valley: geological and geophysical investigations in the lower Romanche valley (Belledonne massif, western Alps)

Olivier Le Roux · Stéphane Schwartz · Jean François Gamond · Denis Jongmans · Pierre Tricart · Michel Sebrier

Received: 8 February 2008 / Accepted: 2 November 2008 / Published online: 20 November 2008

Abstract In the Belledonne massif, the steep Paleozoic Belledonne Middle Fault (BMF) separates micaschists, displaying numerous landslides, from amphibolites. The massif is incised by the lower Romanche river valley. When crossing the BMF, the valley widens into a lozenge-shaped basin recently interpreted as an active pull-apart type structure associated with a major N110 striking Quaternary fault. Multidisciplinary investigations were carried out in the basin to check if this model has implications on the seismic and landslide hazard assessment. This study demonstrated the existence of a N80 sinistral strike slip Séchilienne Fault Zone (SFZ). This fault zone is suspected to offset the BMF by 375 m across the basin. Geophysical experiments revealed that the bedrock depth increases strongly in the basin, up to 350 m. Our study invalidates the active pull-apart origin of the basin and suggests it results from Quaternary glacial and fluvial erosion processes, magnified by the intersection of two inherited structures, the BMF and the SFZ.

Keywords Western Alps · Alpine valley · Alluvial lozenge-shaped basin · Geophysical prospecting · Quaternary erosion processes

O. Le Roux · S. Schwartz · J. F. Gamond · D. Jongmans
Laboratoire de Géophysique Interne et Tectonophysique (CNRS, UMR 5559), Observatoire des Sciences de l'Univers, Université Joseph Fourier, BP 53, 38041 Grenoble cedex 09, France

P. Tricart
Laboratoire de Géodynamique des Chaînes Alpines (CNRS, UMR 5025), Observatoire des Sciences de l'Univers, Université Joseph Fourier, BP 53, 38041 Grenoble cedex 09, France

M. Sebrier
Laboratoire de Tectonique (CNRS, UMR 7072), Université Pierre et Marie Curie-Paris VI, 4 Place Jussieu, 75252 Paris Cedex 05, France

S. Schwartz (✉)
LGIT Rue de la Piscine, BP 53, 38041 Grenoble Cedex, France
e-mail: stephane.schwartz@ujf-grenoble.fr

Introduction

The Belledonne massif, one of the Paleozoic external crystalline massifs of the French Alps (Fig. 1a), extends over more than 120 km in a N30 direction. Mountains of the massif elevation exceed 3,000 m and are bounded to the west by the large topographic depression of the Isère valley (Fig. 1b). The Belledonne massif was part of Hercynian orogen located along the margin of the former European platform. Its basement is constituted by a complex of different metamorphic rocks (gneisses, amphibolites and micaschists), of Precambrian to Carboniferous age, which were deformed and metamorphosed during the Hercynian orogenesis (Ménot 1988; von Raumer et al. 1993). This substratum is covered by non-metamorphic detrital sediments ranging from late Carboniferous to Permian age, and unconformably covered by Mesozoic sediments. During the Alpine orogenesis, the Belledonne massif was affected by crustal shortening associated with the development of metamorphic overprint in greenschist facies conditions in the deep parts of the massif (Goffé et al. 2004). The shortening generated the uplift of the basement and the transportation of the Mesozoic cover to the north-west onto a more external position building-up the Chartreuse and Vercors subalpine chains (Fig. 1b). The Belledonne massif is divided into two major tectonic domains, the external domain to the west and the internal

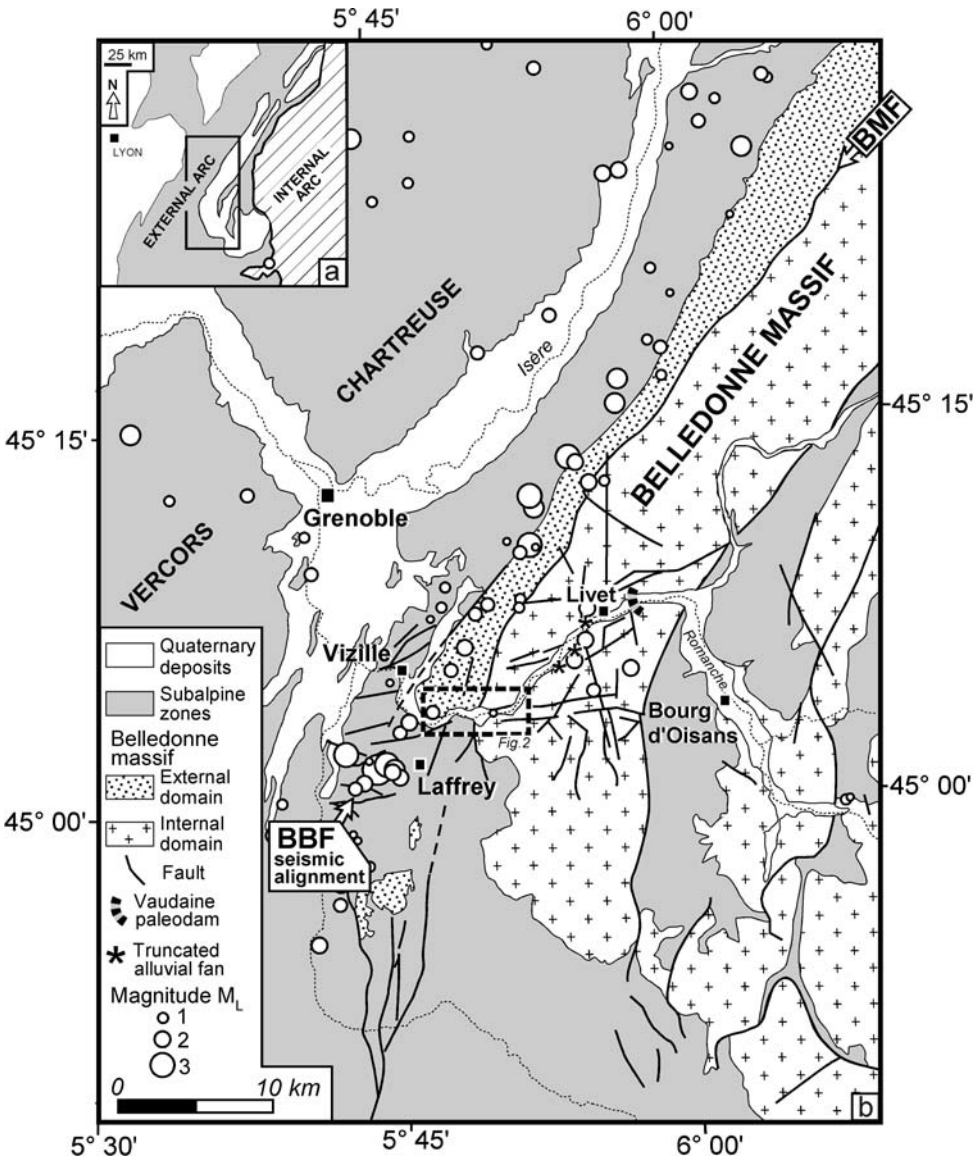

Fig. 1 **a** Structural sketch map of the western Alps with the internal and external arc. **b** Structural and seismicity map of the southwestern part of the external crystalline massif of Belledonne centred on the lower Romanche river valley. The seismic alignment of the Belledonne Border Fault (BBF) and the Belledonne Middle Fault (BMF) are indicated. The polygon in *dashed line* locates Fig. 2

one to the east. These two blocks are separated by a major Late Paleozoic sub-vertical fault, the so-called Belledonne Middle Fault (BMF) (Fig. 1b). On either side of this fault, the two blocks show different lithological content, age and tectono-metamorphic history. The external domain is made of a metasedimentary unit with unknown age corresponding to micaschists affected by polyphased low-grade metamorphism (Fernandez et al. 2002), while the internal domain is constituted by a tectonic stack of acid and basic amphibolitized Cambrian to Devonian rocks (Guillot and Ménot 1999).

The Belledonne massif is affected by a recurrent active deformation, demonstrated by the historical seismicity and the recently acquired seismic and geodetic data. The localisation of the seismic sources, provided for more than 10 years by the Sismalp seismological network, shows a concentration of earthquakes along an axis parallel to the western edge of the massif (Thouvenot et al. 2003). This alignment of seismic events with M_L magnitudes lower than 3.5 and located at shallow depths (less than 10 km) extends on more than 50 km (Fig. 1b). The focal solutions reveal a dextral strike-slip seismo-tectonic regime. This seismic activity restricted below the western limit of the Belledonne massif is suspected to reflect the tectonic activity of the so-called Belledonne Border Fault (BBF) (Thouvenot et al. 2003). However, this structure was never directly observed on the surface through geological or morphological features, although it is correlated with a somewhat flatter topography corresponding to the Aalenian argilite monocline of the Belledonne border hills (Thouvenot et al. 2003). At the southern tip of the BBF, south of the village of Vizille (Fig.1b), a $M_L = 3.5$ earthquake occurred in Laffrey in 1999. The aftershocks were distributed along a N122 alignment perpendicular to that of

the BBF with focal mechanisms corresponding to a left-lateral strike-slip movement (Thouvenot et al. 2003). These two seismic alignments can be interpreted as two conjugate faults consistent with a 3–5 mm/year for compression/strike-slip deformation in the western Alps external domain (front of the Belledonne massif), as shown by GPS monitoring (Martinod et al. 1996, 2001).

The southern part of the Belledonne massif is carved by the east–west trending lower Romanche river valley (Fig. 1b). This incision results from the alternate activity of the Romanche river and the Romanche glacier during the Quaternary glaciations (Montjuvent and Winistorfer 1980). The resulting morphology displays steep slopes, around 35–40°, which are affected by large active or past gravitational movements in the micaschists (Barféty et al. 1970; Fig. 2a). Of major concern is the large Séchilienne landslide which is located on the right bank of the Romanche river and whose more active part corresponds to several million m^3 (Meric et al. 2005). The proposed destabilisation mechanism (Vengeon et al. 1999; Pothérat and Alfonsi 2001) is a slope decompression that follows the ice melting during the last retreat stage of the Romanche glacier at the end of the Würm period (15,000 years BP).

Since the beginning of the glacier retreat (18,000 years BP), four successive lakes were created upstream the Livet gorge (Fig. 1b) by the damming of the Romanche river and flooded the Bourg d'Oisans plain (Bailly-Maître et al. 1997). The last lacustrine episode started about 3,000 years BP, when the valley was dammed by the two opposite alluvial fans of the Vaudaine and the Infernet torrents (Fig. 1b). This heterogenous dam regularly failed, generating gigantic flash floods in the Romanche valley. The last historically known catastrophic flood occured in 1219 and damaged the Grenoble city, 30 km downstream (Cottes 1924). More recently, a minor flooding was reported in 1612. These successive flooding episodes formed the blocky terrace levels observed in the Livet gorge upstream the Séchilienne village (Fig. 1b) (Bailly-Maître et al. 1997) and truncated three large alluvial fans, generating rectilinear scarps up to several hundreds of metres long and several tens of metres high (Fig. 1b).

Close to the village of Séchilienne, the Romanche valley is crosscut by the north–south trending BMF that correlates morphologically with two valleys displaying contrasted features (Fig. 2a). North of the Séchilienne basin, the BMF trace follows a narrow valley. On the contrary, the southern valley is wider and filled by moraines and nested alluvial cones deposited by the Saint Barthélemy torrent (Fig. 2a). The morphological study of the area also reveals a particular kilometric lozenge-shaped basin, so-called the Séchilienne basin, located at the intersection of the lower Romanche valley with the BMF morphological trace (Fig. 2a). The basin is filled by glacio-alluvial deposits of unknown thickness. Based on its lozenge shape morphology, the Séchilienne basin has been interpreted by Pothérat and Alfonsi (2001) as an active pull-apart type structure. According to this hypothesis transtension was supposed to concentrate within a left-hand relay along a N110 sinistral transcurrent fault during Quaternary times. Alternatively, the Séchilienne basin could also have formed by the combined erosion of the Romanche glacier and river on the inherited fracture pattern of the site. The new geomorphological, structural and geophysical data brought in this paper favour this second hypothesis.

Structural and geomorphological analysis

The study of brittle structures along the lower Romanche valley was first performed at the regional scale by using stereographic couples of aerial views (2003 IGN survey). The main regional scale lineaments reported in rose diagrams (Fig. 3) have directions similar to local scale fracturing and are interpreted as faults on either side of the BMF. The dataset was treated according to the two main distinct lithological domains present in the area (Fig. 2b). In the micaschist domain, due to the thick vegetal cover and the presence of large gravitational movements, the observation of the main lineaments is made difficult. Each of the two rose diagrams (Fig. 3) shows a major fracture family with an orientation of N60 in the micaschists and N70 in the amphibolites. In the micaschists a second fracture family, striking N40, is visible. Minor fractures, which are more scattered in the amphibolites than in the micaschists, exhibit a common N140 orientation for the two lithologies. Obviously, the regional scale faulting does not explain the N110 striking morphological boundaries of the Séchilienne basin. In order to solve this paradox, the brittle structure was analysed at the outcrop scale along the boundaries of the basin. Five main measurement sites were defined: sites 1, 2 and 3 in the eastern amphibolites, sites 4 and 5 in the western micaschists (Fig. 3).

The amphibolitic rock bar on the right bank (Fig. 3, site 1) exhibits numerous near-parallel vertical fault surfaces trending N80. They correspond to successive cliffs of several hundred meters in elevation and length. These fault surfaces display near-horizontal striae and grooves reaching several tens of metres length and bear fibres constituted by minerals such as chlorite, epidote and quartz. This paragenesis is symptomatic of greenschists facies conditions suffered during the Alpine deformation and suggests a minimal equilibrium temperature of 200°C (Spear 1993). Such a temperature implies that the main displacement along the fault occurred at several kilometers depth. This depth is not compatible with the near surface deformation process as expected in the Quaternary pull-

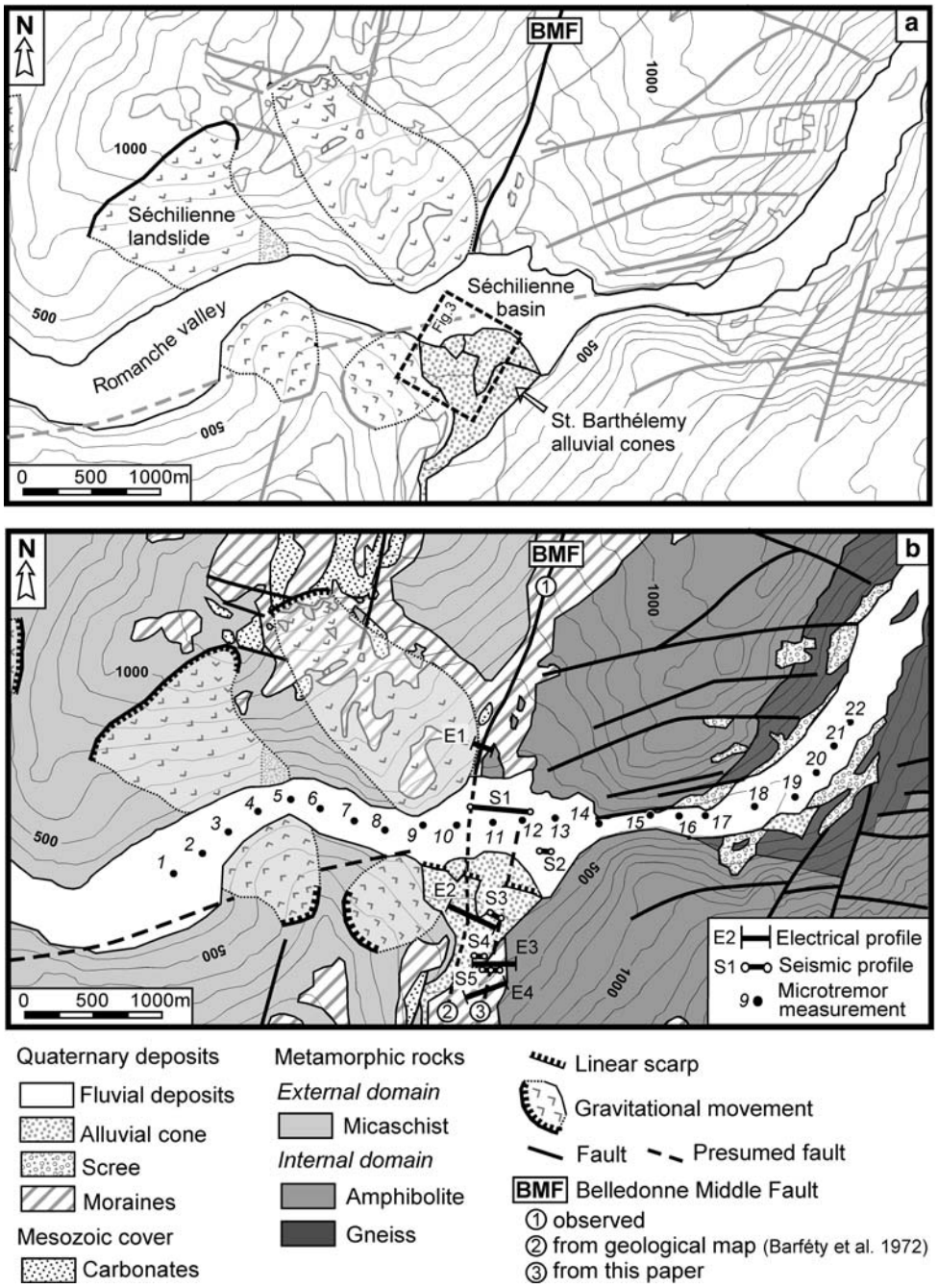

Fig. 2 **a** Geomorphological map of the study area along the lower Romanche valley. The *polygon* in *dashed line* locates Fig. 3. **b** Geological map of the lower Romanche valley (modified from Barféty et al. 1972) with the location of our geophysical investigation

apart basin hypothesis. These main greenschist fibres are locally overprinted by smaller striae (centimetric to millimetric length) that indicate some minor reactivation of the transcurrent fault surface. The main fibres give evidence of a left lateral displacement and they correspond to the main structural direction observed at the regional scale (Fig. 3, rose diagram). Dense faulting and developed friction structures lead us to recognize a major N80 fault zone in the lower Romanche valley. We propose to call this fault the Séchilienne Fault Zone (SFZ on Fig. 3). The morphology of the valley in this place, very narrow, rectilinear along the N80 direction and with vertical walls, is the outward trace of the SFZ. This fault clearly visible in the amphibolites (site 1 in Fig. 3) is expected to connect with the N80 presumed fault crosscutting the micaschists of the left bank of the river, downstream the Séchilienne basin (Fig. 2b). The total length of the structure would exceed 6 km (Fig. 3). Processing striae and striated planes data in amphibolites (sites 1, 2 and 3 in Fig. 3) with the right angle dihedra method (Angelier and Mechler 1977) yielded paleotensors (Table 1). In site 1, a near-vertical intermediate stress axis (transcurrent type regime) and a

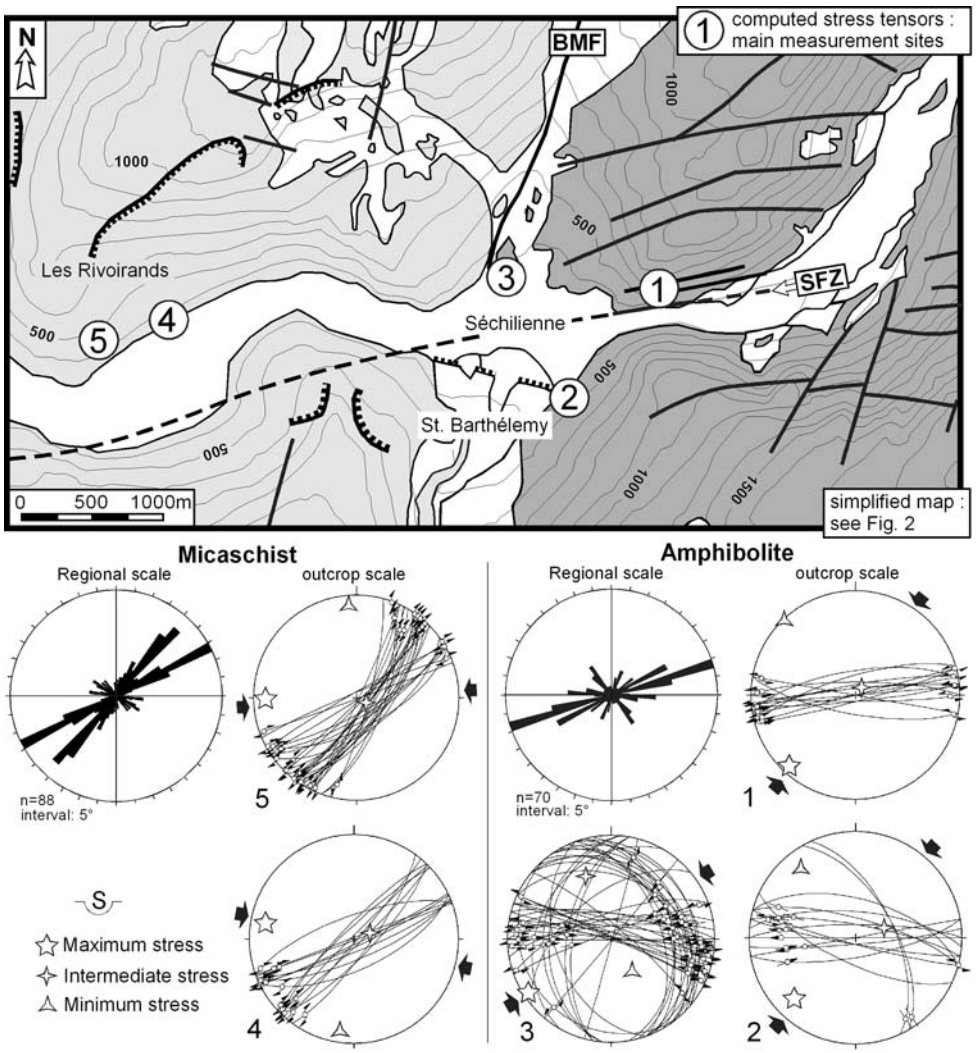

Fig. 3 Location map of the structural analysis sites and of the Séchilienne Fault Zone (SFZ). The regional scale structural data are shown as rose diagrams segmented in 5° classes for the micaschists and the amphibolites. The local scale structural data (at sites labelled 1–5) are plotted as *great circles* on lower hemisphere Wüllf net projection. The paleomain stress axes in each site have been computed by right angle dihedra method. See text and Table 1 for discussion

Table 1 Parameters of the computed paleotensors related to the striated faults along the Romanche river valley

N	Site	*X* (m)	*Y* (m)	*Z* (m)	Nb	$\sigma 1$(°)	$\sigma 2$ (°)	$\sigma 3$ (°)
Amphibolite								
1	RN91 Est	724,125	4,993,500	390	16	219/03	49/87	309/01
2	Saint Barthélémy	723,400	4,992,250	500	15	223/16	088/68	317/15
3	Séchilienne Nord	722,800	4,993,200	360	48	239/03	330/22	140/68
Micaschist								
4	RN91 Ouest	724,125	4,992,250	325	15	281/08	068/80	190/05
5	Les Rivoirands	719,600	4,992,410	370	31	268/06	148/78	359/10

N number of the measurement site, *Nb* number of data, $\sigma 1$, $\sigma 2$, $\sigma 3$ main stress axis (azimuth/plunge)

N35 near-horizontal maximal stress is obtained. In sites 2 and 3, the N80 sinistral strike-slip faulting may also be observed, but it does not correspond to major fault planes like in site 1. Moreover, in sites 2 and 3, numerous small N110 faults are associated with minor N150 low-angle reverse faults. These three computed paleotensors (Table 1) display a N30–N40 near-horizontal maximal stress axis. A permutation of the intermediate and minimal stress axes between site 2 and site 3 results from the relative weight of the numerous low angle reverse fractures in site 3. Based on this analysis, we do not recognize along the right bank of the Séchilienne basin any signature of a major N110 fault zone, as required in the pull-apart basin hypothesis.

In the western micaschists (Fig. 3, sites 4 and 5) striated near-vertical faults are distributed in two main families oriented N40 and N60 and show right lateral displacement. Unlike the amphibolites, these striated faults present weak lateral extension and do not correspond to major topographic cliffs. Moreover, the quartz and calcite fibres as well as the grooves exhibit only centimetric lengths. The inferred paleotensors (Table 1) correspond to a N80–N100 near-horizontal maximal stress and a near-vertical intermediate stress.

In each lithology, the paleotensors inferred from fracturing measurements are homogeneous but differ on either side of the BMF. Nevertheless, they stay compatible with the main direction of the shortening that resulted in the Tertiary regional fold system of Vercors and Chartreuse subalpine chains (Gratier et al. 1989; Gamond 1994). In the amphibolites, the three paleotensors are similar and compatible with a left lateral strike slip displacement along the N80 SFZ. In site 1, fracturing is the signature of the SFZ. In sites 2 and 3, farther from the main fault zone, this SFZ direction is shaded off within a more scattered fracture pattern. In the micaschists, where sites 4 and 5 are far from the presumed trace of the SFZ, the structural data do not show any influence of this fault zone activity.

On the left bank of the Romanche River, the St Barthélemy torrent generated nested post-würmian alluvial fans (Barféty et al. 1972), the presence of which prevents from precisely locating the BMF trace (Fig. 2). The main fan (cone 1, Fig. 4), which is the oldest one and is stabilized, show a lateral kilometric extent with a slope less than 5°. The frontal part of this fan is truncated by a rectilinear 1,000-m-long N110 trending scarp that makes the southern boundary of the Séchilienne basin. This limit corresponds to a steep slope break (>50°) that can reach 25 m height in its central part (Fig. 4). This bench is carved by two more recent fans. The smallest one (cone 2, Fig. 4), 150 m wide, is also stabilized and partially truncated by a N110 trending 50 m long and 3 m high scarp. The central part of the bench is overlaid by the present-day St Barthélemy alluvial fan (cone 3, Fig. 4) that spreads out in the Séchilienne basin over more than 500 m wide. On the contrary, the northern boundary of the Séchilienne basin does not display any alluvial fan. The bare amphibolitic bedrock of this side is composed by an association of small scale fractures of varied orientation (N80, N110, N150). This association makes its contour line jagged while the global envelope trends N110 (Fig. 3) and parallels the southern limit of the basin. This particular frame gives the basin its lozenge shape. To explain the basin morphology two hypotheses can be proposed. (1) Quaternary tectonic processes associated with a pull-apart displacement (Pothérat and Alfonsi 2001) and causing the subsidence of the basin infilling. (2) Quaternary erosion activities of the Romanche glacier and river reworking a previously faulted zone at the contact between two different lithologies.

Geophysical prospecting

Geophysical experiments were performed in and around the Séchilienne basin, in order to discriminate between the two hypotheses for the basin formation. A first objective was to locate the BMF south of the basin where it is hidden below Quaternary deposits and to assess if this inherited linear structure is displaced across the basin. A second objective was to determine the longitudinal valley floor profile across the basin.

Methods

Near-surface geophysical prospecting has now become a major tool, particularly in active tectonics, for constraining the geometry of faults affecting the shallow layers (among others, Demanet et al. 2001; Green et al. 2003; Carvalho et al. 2006). The choice of the investigating technique mainly depends on the expected geophysical contrast, the target depth and the required resolution. A fault generally juxtaposes blocks of different nature and may also disturb hydrogeological conditions. Since the electrical resistivity is a geophysical parameter exhibiting a wide range of values depending on the nature of the material and the water content (Telford et al. 1990). Electrical Resistivity Tomography (ERT) has emerged as one of the more frequently used and robust techniques for tracing faults at the surface from a few metres to a few tens of metres of depth (e.g. Suzuki et al. 2000; Demanet et al. 2001; Caputo et al. 2003; Nguyen et al. 2007). Faults are, however, often buried below a recent soil cover and the high resolution seismic reflection technique was used for mapping faults at greater depth, from few tens to few hundreds of metres (e.g. Shields et al. 1997; Demanet et al. 2001; Carvalho et al. 2006). Sedimentary basins (from a few tens of metres to a few kilometre thick), are classically imaged using the seismic reflection technique (e.g. Whiteley et al. 1986; Stephenson et al. 2002; Bradford et al. 2006) that also allows to image the bedrock interface (Brabham and McDonald 1992; Jongmans et al. 1998). Since the pioneering work of Nogoshi and Igarashi (1972) and Nakamura (1989), the recording of microtremors has been increasingly applied for investigating sedimentary structures. In particular, the *H/V* technique, which consists in computing the spectral ratio of the Fourier amplitude spectra of the horizontal (*H*) over the vertical (*V*) components of the microtremors recorded at the surface, was shown to be able to provide a reliable estimate of the fundamental resonance frequency f_0 of the site (Bard

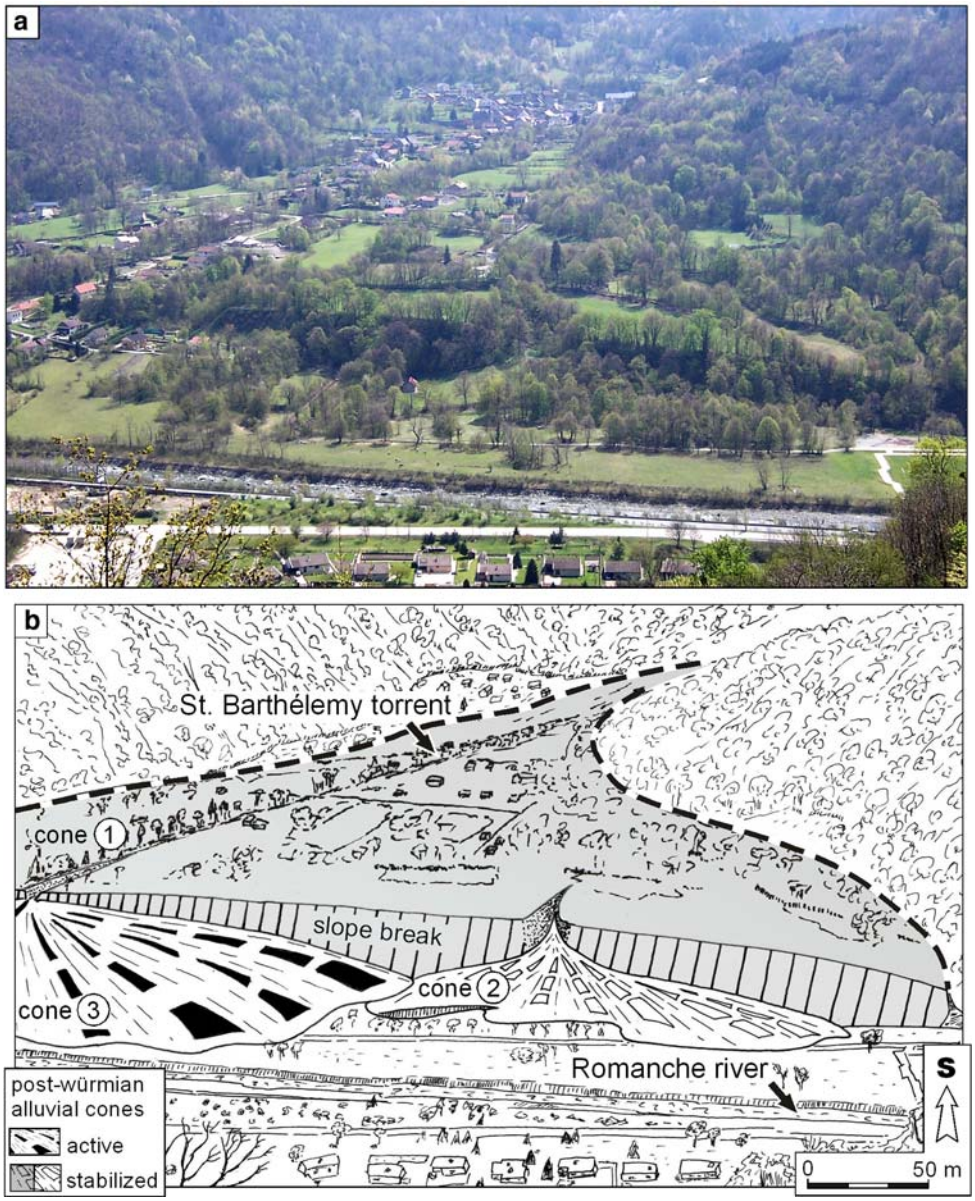

Fig. 4 **a** Southward view of the Saint Barthélemy post-würmian alluvial system seen from north. The area photographed is located on Fig. 2a. **b** Interpretation of the alluvial system as three *nested cones*. The stabilized cone 1 displays a rectilinear slope break

1998). Because of the relation between f_0, shear wave velocity within the soft layers and their thickness (Tokimatsu 1997), the *H/V* method was applied as an exploration tool for mapping the geometry of different basins (e.g. Delgado et al. 2000; Parolai et al. 2002; Guéguen et al. 2007), assuming that the shear-wave velocity profile is known. These three geophysical methods were applied in this study in order to define the position of the BMF and to estimate the thickness of the infilling of the Séchilienne basin.

Four ERT profiles (labelled E1–E4, Fig. 2b) were performed using a Wenner configuration with a number of electrodes ranging from 64 to 80 and a spacing of 2.5 or 5 m. The electrical profile characteristics are summarized in Table 2. Apparent resistivity data were inverted using the algorithm proposed by Loke and Barker (1996) using the software Res2dinv (Loke 1998). Five seismic profiles (S1 to S5) with various characteristics (Table 3) were acquired in the Sechilienne Basin (S1 and S2) and in the St Barthelemy alluvial fan (S3–S5) (Fig. 2b). For profiles S1 and S3–S5, the classical *P*-wave refraction method (Burger 1992) was used to derive *P*-wave velocity values and the geometry of the layers. The signals of the long (470 m) profile S1 were recorded with 4.5 Hz geophones and the dispersion curves of the Rayleigh waves were computed and inverted for deriving the *S*-wave velocity profile. Surface wave inversion was performed using the *Geopsy* software (http://www.geopsy.org; Wathelet 2003). Reflected events were also picked and processed using the formula of Dix (1955) in order to obtain a vertical *Vp*

Table 2 Physical parameters of geophysical experiments: Electrical profiles

Profile	Ne	Xe (m)	*L* (m)	*D* (m)
E1	64	2.5	157.5	25
E2	80 + 16	5	475	65
E3	64	5	315	50
E4	80	5	395	65

E2 was performed using the roll-along technique with one cable of 16 electrodes

Ne number of electrodes, *Xe* electrode spacing, *L* profile length, *D* approximate investigation depth

Table 3 Physical parameters of geophysical experiments: seismic profiles

Profile	Ns	Ng	Xe (m)	*T* (s)	*F* (Hz)
S1	5	48	10	5	2,000
S2	2	24	2.5	2	2,000
S3	5	24	2.5	2	2,000
S4	5	24	4	2	2,000
S5	10	24	5	2	2,000

Ns number of sources, *Ng* number of geophones, *Xg* geophone spacing, *T* time length, *F* sampling frequency

profile in the basin. Profile S2 is a short SH refraction profile performed in the basin for obtaining *S*-wave velocity values in the shallow alluvial layers. Microtremors were recorded at 22 sites spaced 250 m apart along the Romanche valley (Fig. 2). Acquisition was made during 30 min with a three-component 5-s sensor and a sampling frequency of 200 Hz. The records are cut in time windows of 30 s and the Fourier amplitude spectra are computed and smoothed using the processing proposed by Konno and Ohmachi (1998). The *H/V* ratio at each station is obtained by averaging the *H/V* ratios of all windows.

Position of the Belledonne Middle Fault (BMF)

Four ERT profiles (E1–E4, Fig. 2b) were performed on both sides of the basin in order to locate the BMF to the south of the Séchilienne basin, where it is hidden by Quaternary deposits. BMF juxtaposes micaschists to the west and amphibolites to the east (Fig. 2b), which are likely to exhibit a strong contrast of electrical resistivity. The four profiles were obtained after five iterations (Fig. 5) with Root Mean Square (RMS) values lower than 3%. The inferred models are therefore consistent with the data. Profile E1 was carried out to the North of the Séchilienne basin (Fig. 2b), where the position of the BMF is well constrained by geological outcrops. Below a 3–10-m thick resistive layer (a few thousands ohm m), interpreted as rock debris, the BMF is clearly evinced by a sharp lateral contrast of resistivity, from 400 to 1,000 ohm m in the micaschists to more than 3,000 ohm m in the amphibolites. The resistivity value measured in the micaschists is consistent with the results found in the same rocks close to the Séchilienne landslide (Meric et al. 2005). Directly south of the Séchilienne basin, the bedrock is covered by the Quaternary alluvial fan where the village of Saint Barthélemy is installed. One 480-m-long electrical resistivity profile and one 57.5 m long seismic profile (E2 and S3, Fig. 2b) were performed on this alluvial fan in order to determine the fan thickness and to locate, if possible, the BMF underneath. The 60-m-deep electrical image E2 (Fig. 5b) shows little resistivity contrast with values ranging between 400 and 800 ohm m on average. Only local resistive spots are observed as well as a complex-shape conductive zone below the stream flowing over the fan. The seismic profile S3 performed at the eastern end of E2 (Fig. 2b) reveals the presence of three seismic near horizontal layers with *P*-wave velocity values of 750, 1,500 and 3,200 m/s (Fig. 5b). The two-first layers probably correspond to the alluvial fan material with the presence of the water table (1,500 m/s) at about 14 m depth. The high velocity ($Vp = 3{,}200$ m/s) measured in the third layer indicates that the bedrock top is reached at 30 m depth. Similar *Vp* values were found in the micachists by Meric et al. (2005) on the other bank of the Romanche River. Resistivity values (400–800 ohm m) below 30 m are consistent with the presence of micaschists and do not show a lateral contrast. These results suggest that the about 30 m thick alluvial fan is made of partially saturated to saturated medium-size material overlying micaschists with similar resistivity values. The BMF is thus not seen on the electrical image and the contact between micaschists and amphibolites has so to be eastwards located. Two other electrical tomography sections (E3 and E4) were conducted to the South of the Séchilienne basin (Fig. 2b), where BMF is buried below thin till deposits. The eastern ends of the two profiles were positioned on the amphibolites. On the E3 section, below the resistive moraine layer (over 2,000 ohm m with some high resistivity zones probably due to the presence of pebbles and boulders in the moraine), the image (Fig. 5c) exhibits a sharp lateral increase of resistivity from the west (500–800 ohm m) to the east (more than 2,500 ohm m). The superficial conductive zone (less than 600 ohm m) observed between 140 and 180 m of distance corresponds to the location of a spring at 160 m characterized by a conductive water (measured around 25 ohm m) which locally decreases the ground resistivity. Two seismic profiles were performed along this E3 section: S4 at the western end of E3 and S5 centred over the spring (Fig. 5c). The seismic refraction interpretation reveals the presence of three layers with *P*-wave velocity values of

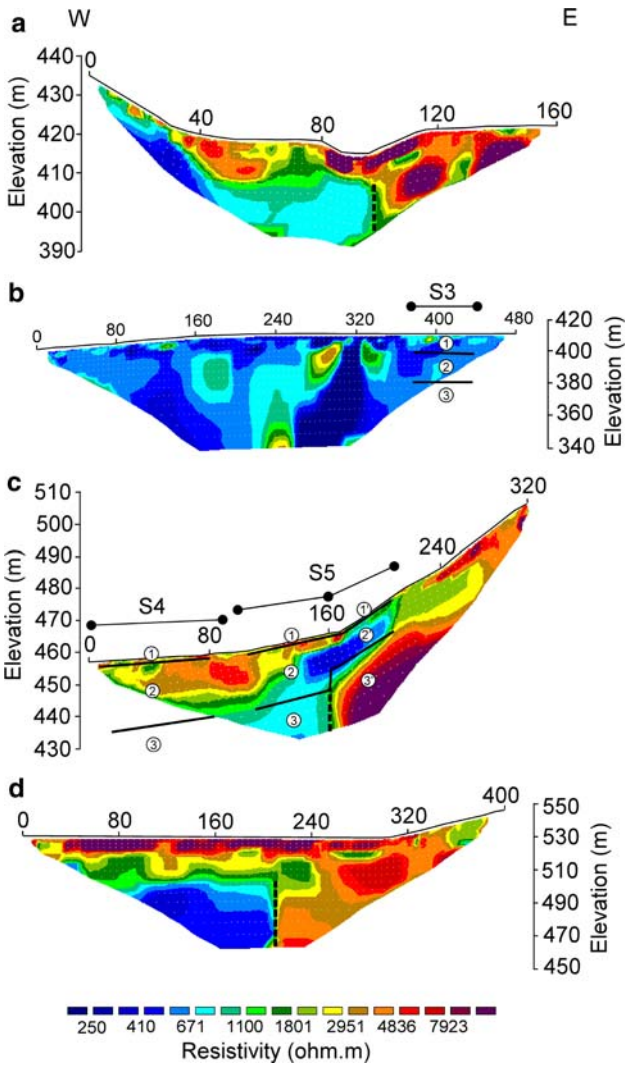

Fig. 5 West–East oriented ERT sections with seismic refraction interpretation of S3, S4 and S5 profiles. **a** E1 resistivity profile, RMS = 3.2%, five iterations. **b** E2 resistivity profile, RMS = 2.3%, five iterations, *P*-wave velocity deduced from seismic refraction interpretation of profile S3: (*1*) 600–800 m/s (*2*) 1,450–1,550 m/s (*3*) 3,100–3,300 m/s. **c** E3 resistivity profile, RMS = 2.0%, five iterations, *P*-wave velocity deduced from seismic refraction interpretation of profile S4 and S5: (*1*) 350–400 m/s (*2*) 900–1,100 m/s (*3*) 3,150–3,250 m/s (*1′*) 300–350 m/s (*2′*) 700–800 m/s (*3′*) 4,300–4,700 m/s. **d** E4 resistivity profile, RMS = 2.3%, five iterations. *Dotted line* deduced position of the Belledonne Middle Fault (BMF)

350, 1,000 and 3,200 m/s west of the spring, and 350, 700 and 4,500 m/s east of the spring (Fig. 5c). The overlying soil layers are characterized by low *P*-wave velocity (less than 1,000 m/s) suggesting that these layers are unsaturated, in agreement with the relative high-resistivity values (over 650 ohm m) measured along profile E3 (Fig.5c). The bedrock top is reached between at 20 m to 30 m depth to the west of the spring and at 10 m depth eastwards. This 10-m high step, associated at depth with significant lateral velocity and resistivity contrasts (from 3200 m/s and 650 ohm.m to the west to 4500 m/s and 2500 ohm.m to the east, Fig.5c), is interpreted as the trace of the BMF juxtaposing micaschists and amphibolites. On the E4 section, the electrical image (Fig.5d) also exhibits a sharp lateral increase of resistivity from the west (400–700 ohm.m) to the east (more than 2500 ohm.m) at 30 m depth. The very high resistivity values (more than 8000 ohm.m) obtained in the first five meters coincide with the presence of amphibolites blocks having fallen from the eastern slope. Below, the high resistivity values (1000–4000 ohm.m) measured down to 30 m depth probably correspond to unsaturated quaternary deposits (till) with the presence of pebbles and boulders. The strong lateral resistivity contrast at depth is also interpreted as the trace of the BMF.

Geophysical results show that the BMF is shifted 200–300 m to the east (Fig. 2b, trace 3) compared to the fault trace 2 drawn on the geological map (Barféty et al. 1972). Considering a rectilinear geometry for the southern and northern branches of the BMF (trace 3 in Fig. 2b) gives a sinistral strike-slip displacement of about 375 m in the centre of the basin, which could result from the activity of the SFZ.

Basin investigation

Twenty-two single-station microtremor measurements were made along the Romanche valley, downstream, into and upstream the Séchilienne basin (labelled 1–22 in Fig. 2b). Three *H/V* curves (stations 4, 12 and 16) and a section with the 22 *H/V* ratios are plotted in Fig. 6. The computed *H/V* curves exhibit two specific shapes according to the position of the stations. First, downstream (Fig. 6a and d) and upstream (Fig. 6c, d) the Séchilienne basin, *H/V* ratios show a well defined single peak with an amplitude greater than 4 between 1.4–2 and 2–3.5 Hz, respectively. The curve shape fits the criteria proposed in the SESAME guideline (Koller et al. 2004) for a 1D resonance phenomenon and the peak frequency values correspond to the resonance frequency of the alluvial layers overlying the bedrock. Downstream the basin, the peak frequency decreases from 2.5 to 1.5 Hz (Fig. 6d), indicating a deepening of the bedrock top. Less frequency variations are shown upstream where the highest peak frequency values are reached (around 3 Hz). Into the Séchilienne basin (Fig. 6b, d), *H/V* ratios do not display a well-defined peak with an amplitude higher than 3 over a wide low-frequency band (0.3–1.5 Hz) in the centre of the basin and a steady low *H/V* value (<2) near the basin borders. Such plateau-like shapes were already observed on many valley or basin edges where significant variations of the soft layer thickness occur (Uebayashi 2003; Koller et al. 2004). Guillier et al. (2006) simulated ambient seismic noise in 2D and 3D structures in order to test the relevancy of *H/V* curves in

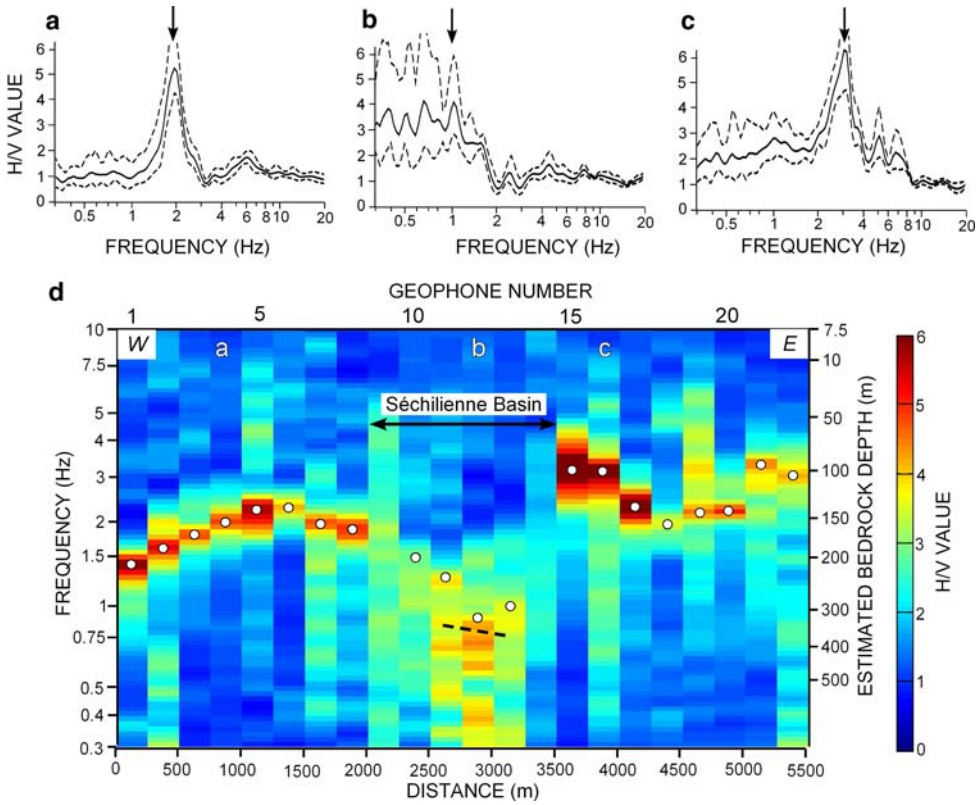

Fig. 6 *H/V* curves at **a** Station 4 (downstream the basin), **b** Station 12 (within the basin) and **c** Station 16 (upstream the basin). The *arrows* show the peak frequency. **d** Longitudinal *H/V* profile along the river. *White circle* peak frequency. *Dashed line* interface between sediments and bedrock as inferred from seismic reflexion

providing qualitative and quantitative information on site features. They showed that *H/V* curves exhibit well-defined peaks in the flat parts of the structures and plateau-like shapes of low amplitude in parts with strong lateral sediment thickness variation. For such plateau-like *H/V* curves, picking the frequency at the plateau cut-off (Fig. 6b) generally overestimates the 1D theoretical resonance frequency, resulting in a lower bound of the bedrock depth value.

Two seismic profiles were conducted in the Séchilienne basin (S1 and S2 in Fig. 2b) in order to characterize the seismic velocities in the glacio-alluvial layers and to determine the basin depth. Figure 7a shows the vertical-component seismograms recorded along the 470-m-long S1 profile for the offset shot T5. They exhibit predominant Rayleigh-type surface waves (*R*) which will be used further for deriving *S*-wave velocity values. Refracted *P*-waves were first analysed and the time-distance graphs for the direct and reverse shots (T2 and T4) are plotted in Fig. 7b. They show the presence of three layers with *P*-wave velocity values of about 700, 1,400 and 2,300 m/s, respectively (Fig. 7d). The relatively low velocity ($Vp \approx 2{,}300$ m/s) within the third layer indicates that the bedrock was not reached and probably corresponds to deep saturated glacio-alluvial sediments. The similarity of the curves and of the *P*-wave velocity values for direct and reverse shots indicates that layers are near horizontal. The water table ($Vp = 1400$ m/s) was found at about 8 m depth. The Rayleigh wave dispersion curve was extracted between 5 and 20 Hz and is plotted in Fig. 7c. Phase velocity values vary between 400 m/s at high frequency to 650 m/s at low frequency. This curve was inverted using a three-layer model and the obtained *S*-wave velocity profile is shown in Fig. 7d with *Vs* values of 300, 600 and 850 m/s in the 3 layers. These values are consistent with the results of the SH refraction profile S2 (Fig. 7d). *S*-wave velocity in the shallow layer (4–7 m thick) is about 300 m/s and dramatically increases to reach 650–800 m/s in the consolidated alluvial layers. Similar to the refraction experiment, the surface wave investigation was not deep enough to reach the bedrock. We then attempt to find out reflected events in the measured seismograms using classical processing techniques. Figure 8a shows the signals of shot T5 after applying a 50–100 Hz band pass filter (Fig. 8a). The obtained seismic record reveals four well-defined reflected waves (R1–R4 in Fig. 8a), whose analysis yields the *P*-wave seismic profile of Fig. 8b. The *P*-wave velocity values (2,200–2,500 m/s) are consistent with the ones found in the refraction analysis. R1–R3 events probably correspond to seismic impedance contrasts in the alluvial filling. After normal move-out, the stronger reflection in the seismograms (R4) appears between 300 ms (for shot T1) and 340 ms (for shot T5) TWT, corresponding to depth values between 330 m to the west

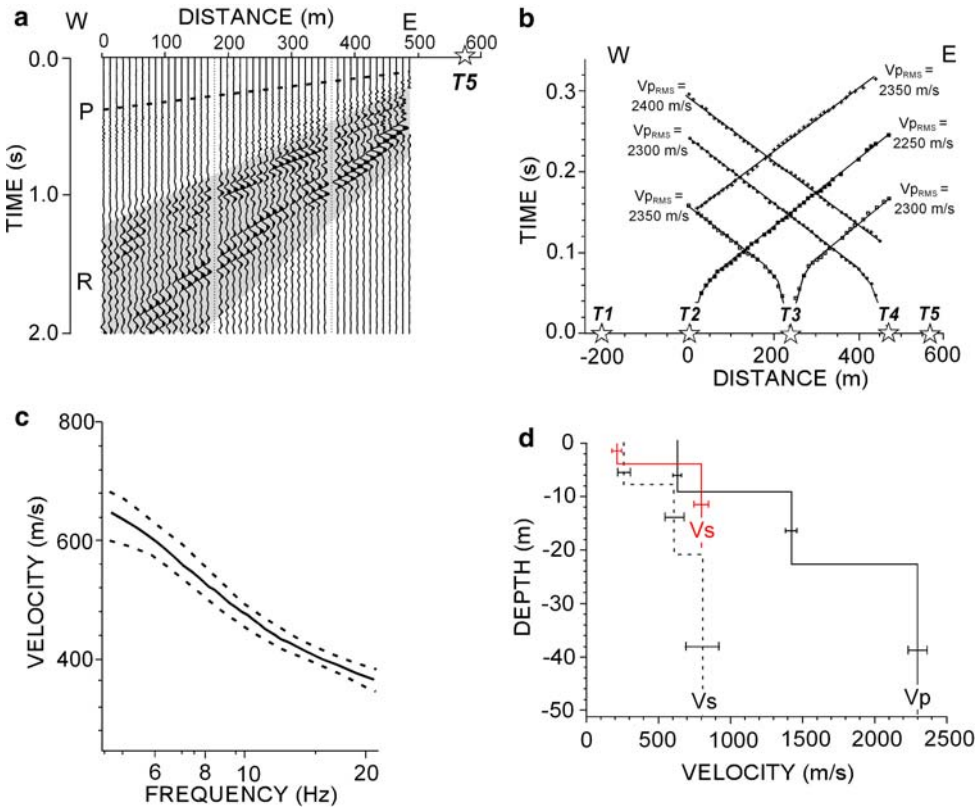

Fig. 7 Seismic investigation in the basin. **a** Raw S1 seismic section of shot T5, *P* refracted *P*-wave, *R* Rayleight waves. **b** Time–distance graph inferred from the five shots of S1 profile. **c** Dispersion curve of surface wave for shot T5. *Dashed lines* show two uncertainties. **d** Interpretative section of velocity inferred from seismic refraction (*continuous line*) and from surface wave inversion (*dashed line*), *dark* S1 profile, *grey* S2 profile

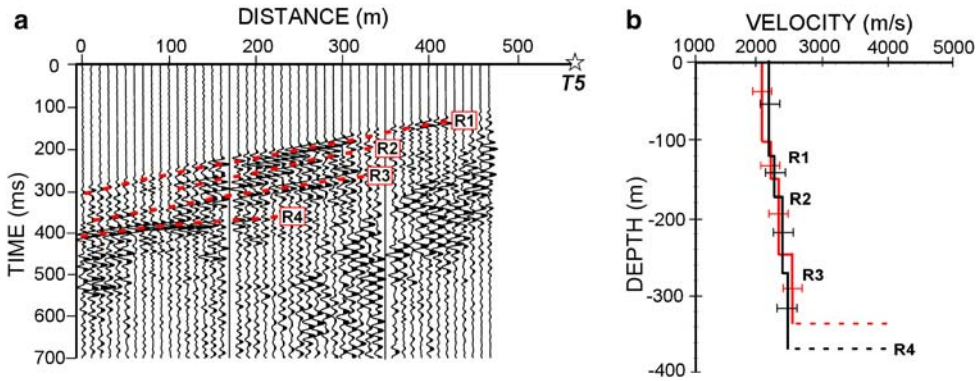

Fig. 8 **a** S1 seismic record of shot T5, processed with a band-pas 50–100 Hz filter. *R1–R4* reflected waves. **b** P wave velocity profile inferred from seismic reflection, *dark* S1 profile shot T5, *grey* S1 profile shot T1

and 370 m to the east (Fig. 8b). This main reflector probably coincides with the interface between the bedrock and the sediments.

In order to evaluate the thickness of the sedimentary deposits along the valley, we have computed the ellipticity curve for 7-layers of 1D velocity models defined from seismic experiments (Fig. 9a). *Vp* and *Vs* values in the first three layers (to 50 m depth) are given by the seismic refraction and surface wave inversion results, while *Vp* values in the three deeper sedimentary layers are provided by the analysis of reflected waves (Fig. 8b). *S*-wave velocities for these layers are derived from *P*-wave velocities, keeping the Poisson's ratio of 0.42 obtained in the third layer. For the *P*-wave velocity in the crystalline substratum, we took the value of 4,000 m/s measured by Meric et al. (2005) at 100 m depth in the micaschists. A corresponding value of 2,000 m/s for *S*-wave velocity was obtained considering a Poisson's ratio of 0.33. Ellipticity curves were computed for five models with sediment thickness *H* increasing from 100 to 400 m. The velocity profiles were linearly adjusted to the bedrock depth, from the second to the seventh layer (Fig. 9a). Ellipticity values are plotted versus frequency in Fig. 9b. For these 1D models, the curves exhibit a clear peak at a frequency, which decreases when the thickness *H* of the glacio-alluvial deposits increases. The comparison between the computed ellipticity curves (Fig. 9b) and the experimental peak frequency values (white dots in Fig. 6d) allows

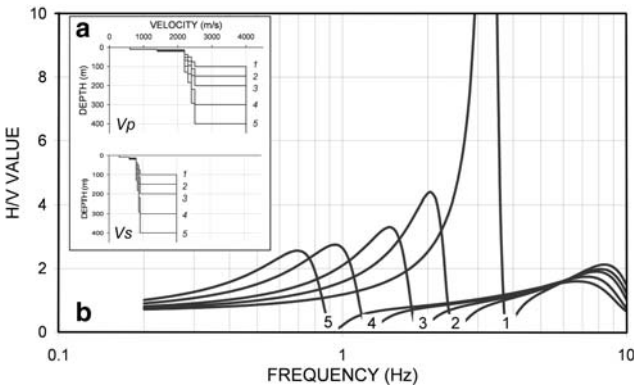

Fig. 9 **a** Velocity profiles for five models with different sediment thickness (*H*). **b** Computed *H/V* curves for different sediment thickness (*H*). *1* $H = 100$ m, *2* $H = 150$ m, *3* $H = 200$ m, *4* $H = 300$ m, *5* $H = 400$ m

sediment thickness values to be estimated below each measurement point (see the depth scale in Fig. 6d). Along the *H/V* profile, the sediments display two zones of increased thickness. East of the profile (geophones 17–20 on Fig. 6d) the sediment thickness reaches 150–170 m. Over the Séchilienne basin (geophones 10–13 in Fig. 6d), the thickness abruptly increases to 300–350 m. In the deeper part of the basin, thickness values obtained from the *H/V* curves are well correlated with the reflector analysis which found the bedrock depth to be between 330 and 370 m (dotted line in Fig. 6d). The striking feature of the basin longitudinal profile is the strong asymmetry with a steeper eastern boundary. This boundary can be interpreted as the superimposition of two cumulative weakening effects: (1) the contact zone between the micaschists and the amphibolites (BMF) and (2) the SFZ trace.

Discussion

The data presented in this paper allow evaluating the consistency of each of the two hypotheses proposed for the basin formation.

Pull-apart activity

This interpretation is based on the lozenge shape of the Séchilienne basin and on the tectonic significance of the N110 trending rectilinear slope break, which affects the oldest alluvial fan (cone 1) of the Saint Barthélemy torrent. In the pull-apart hypothesis (Pothérat and Alfonsi 2001), the slope break would correspond to the southern branch of a dilational jog along a major sinistral strike-slip N110 fault zone, whereas the northern branch would correspond to the present day N110 northern boundary of the Séchilienne basin. Our geological and morphological observations, along the structural measurements at different scales (including on the right bank in the micaschists downstream the Sechilienne basin, site 4), do not, however, confirm the existence of such a N110 major sinistral fault zone. On the contrary, our study has revealed the existence of a left lateral N80 trending strike-slip fault (SFZ, Fig. 3) which could explain the sinistral displacement of about 375 m between the northern and southern branches of the BMF in the centre of the basin. The hypothesis that these two branches can be joined through a virgation is unlikely, as the BMF trace at the regional scale does not exhibit such abrupt geometry changes.

In such a pull-apart model, any increment of displacement along the main fault should create a free space causing the topographic basin surface and the frontal part of cone 1 to subside. Taking into account the present-day basin surface geometry (1000 m × 750 m) and a depth of 350 m (determined from *H/V* and seismic data), a simple computation model based on a constant infilling volume (before and after incremental opening) shows that the N110 horizontal displacement needed to obtain a 25-m subsidence (maximal measured height of the slope break) ranges from 70 m for a rectangular transverse vertical section to 130 m in the case of a triangular transverse vertical section. Since the slope break is dated post-Würm (Barféty et al. 1972), the mean inferred strike-slip velocity is then about 4.5–8.6 mm/year. In the studied area, the potential maximal magnitudes estimated from the historical and the instrumental seismicity recorded during the last 20 years by the Sismalp network ($M_L < 3.5$) are lower than $M_L = 5.5$ (Thouvenot et al. 2003). The scale laws (e.g. Wells and Coppersmith 1994) that express the magnitude versus the displacement at the ground surface show that a $M_L = 5.5$ seismic event would generate a displacement of about 1 cm, whereas a $M_L = 7.5$ seismic event would generate a displacement of about 10 m. In the case of the Séchilienne basin, the 4.5–8.6 mm/year values imply either (1) a recurrent seismic activity corresponding to a $M_L = 5.5$ seismic event per year during a 15,000-year period on a 2-km-long fault rupture surface, or (2) 7–13 seismic events with a $M_L = 7.5$ on a 100-km-long fault rupture surface during the same period of time. None of these two extreme scenarios matches the seismo-tectonic and morphologic features of the area. The Séchilienne pull-apart basin model then appears to be weakly supported by the data. Moreover, in tectonically active zones such as the French south eastern alpine foreland, the estimated Quaternary to present-day deformation rates along the major strike slip faults (like the Middle Durance Fault) show values ranging from 0.01 to 0.1 mm/year (Siame et al. 2004; Cushing et al. 2007). The post Würmian deformation rates resulting from the Séchilienne pull-apart hypothesis are thus not consistent with such low rates.

Quaternary erosion processes

In the Alps the geometry of the valleys results from the combined erosional activity of glaciers and rivers. The glacier effect was to broaden valley bottoms and to generate multiple steps and overdeepenings tens to hundreds of metres deep (MacGregor et al. 2000; van der Beek and Bourbon 2008). Several hypotheses have been put forward for explaining the generation of steps and overdeepenings: variations in glacier length over multiple climate cycles, tributary junctions, variations in lithology or rock resistance and inherited tectonic patterns (MacGregor et al. 2000; Anderson et al. 2006; Molnar et al. 2007). Geophysical measurements performed along the Romanche valley evidence the presence of two overdeepenings in the Romanche floor profile. The upstream shallowest one (150–170 m in depth) is located within the amphibolites at the crossing at depth of the SFZ. It probably results from a selective erosion process led by this fractured zone. The downstream deepest one (about 350 m in depth) is located within the micaschists across the Séchilienne basin and exhibits a strong asymmetry. Its steep eastern boundary corresponds to the contact between amphibolites and the more erodable micaschists, which was shown by geophysical data to be shifted 375 m upstream when compared to the trace drawn in the geological map. This significant bedrock deepening along with the broadening of the valley (Séchilienne basin) probably stems from the strong lithological contrast between amphibolites and micaschists. In this interpretation, the lozenge basin shape results from the glacier and river erosion activity on a heterogeneous and strongly fractured area located at the junction of two inherited fault zones (SFZ and BMF). The rectilinear slope break truncating the post-Würm cone 1 of the Saint Barthélemy torrent is assigned to one of the catastrophic floods along the Romanche valley (Bailly-Maître et al. 1997), resulting from a sudden emptying of the Bourg d'Oisans natural paleo-lake (Fig. 1b). This interpretation is supported by the presence of a similar but smaller scarp affecting cone 2 in the same fan complex (Fig. 4) and by the observation of three truncated alluvial fans upstream the Séchilienne basin (Fig. 1b). The slope break of cone 1 could be due to the last registered catastrophic flood of 1219 and the truncation affecting cone 2 to one subsequent minor event. Chronological data have to be acquired to confirm this hypothesis. The N110 striking northern boundary of the Séchilienne basin does not present a rectilinear global trending. In detail, the contour line is jagged and it was made by a succession of erosion surfaces. These erosive directions follow preferential fracture directions unroofed by the Romanche river activity.

Conclusions

The peculiar lozenge-shaped Séchilienne basin was the subject of a multidisciplinary study combining geophysical, geological and geomorphological investigations. Seismic data (microtremor measurements and reflected waves) revealed a significant valley floor overdeepening (from 100 to 350 m depth) across the Séchilienne basin, exhibiting a strong asymmetry with a steep eastern boundary. This overdeepening is aligned with the southern branch of the near-vertical Late Paleozoic BMF, as located by the ERT profiles. This fault was displaced eastward 375 m with respect to its trace on the geological map. This BMF shift was attributed to a N80 sinistral strike slip fault so-called Séchilienne Fault Zone (SFZ) which was observed on the right bank of the amphibolite gorges just upstream the Séchilienne basin. An overdeepening of the valley floor (from 100 to 170 m) was observed in the eastern prolongation of this fault. No sign of recent activity along this fault was evidenced by our study. Data interpretation suggests that the Séchilienne basin geometry results mainly from the Quaternary glacial erosion across a major lithological contrast, between amphibolites to the east and more erodable micaschists to the west. The rock erodability in the zone was magnified by the intersection of two inherited structures, the BMF and the Sechilienne Fault Zone. The N110 striking northern boundary of the basin does not correspond to any major fault zone. It was formed by a succession of erosion surfaces produced by the Romanche activity and led by the existing fracture pattern. In the southern side of the basin, the N110 rectilinear scarp truncating the post-Würm cone 1 of the Saint Barthélemy nested cones system is interpreted to be due to one of the major floods which occurred along the Romanche valley. The tectonic origin of this scarp was shown to be weakly supported by the seismicity and geological data. In the micaschist domain, the concentration of gravitational instabilities suggests that the landslide hazard assessment may depend on recent Quaternary processes reworking a previously mechanically weakened massif. The scope of this work is that the Séchilienne lozenge-shaped basin was partly controlled by Quaternary glacial and fluvial erosion processes reworking the previous geological and structural framework of the Belledonne massif.

Acknowledgments We thank JD Champagnac and an anonymous reviewer for their helpful suggestions, which improved the quality of the manuscript. This work was financially supported by Pôle Grenoblois des Risques Naturels (PGRN) programme. We gratefully acknowledge T. Camelbeeck for his helpful discussions about the seismic framework.

References

Anderson RS, Molnar P, Kessler A (2006) Features of glacial valley profiles simply explained. J Geophys Res 111:F01004. doi:10.1029/2005JF000344

Angelier J, Mechler P (1977) Sur une méthode graphique de recherche des contraintes principales également utilisable en tectonique et en séismologie : la méthode des dièdres droits. Bull Soc Geol Fr 7:1309–1318

Bailly-Maître MC, Montjuvent G, Mathoulin V (1997) Les quatre ancien lacs de l'Oisans (Alpes françaises du Nord). Rev Geogr Alp 1:33–52

Bard PY (1998) Microtremor measurements: a tool for site effect estimation? Proceeding of the Second International Symposium on the Effects of Surface Geology on Seismic Motion, Yokohama, Japan 3:1251–1279

Barféty JC, Gidon M, Montjuvent G (1970) Extension et importance des glissements superficiels aux abords méridionaux de Grenoble. Geologie Alp 46:17–22

Barféty JC, Bordet P, Carme F, Debelmas J, Meloux M, Montjuvent G, Mouterde R, Sarrot-Reynauld J (1972) Notice explicative, carte géologique de la France (1/50.000), feuille Vizille (797). BRGM, Orléans

Brabham PJ, McDonald RJ (1992) Imaging a buried river channel in an intertidal area of South Wales using high-resolution techniques. Q J Eng Geol 25(3):227–238. doi:10.1144/GSL.QJEG.1992.025.03.06

Bradford JH, Liberty LM, Lyle MW, Clement WP, Hess S (2006) Imaging complex structure in shallow seismic-reflection data using prestack depth migration. Geophysics 71(6):175–181. doi:10.1190/1.2335659

Burger HR (1992) Exploration Geophysics of the Shallow Subsurface. Prentice Hall, New Jersey, pp 1–489

Caputo R, Piscitelli S, Oliveto A, Rizzo E, Lapenna V (2003) The use of electrical resistivity tomographies in active tectonics: examples from the Tyrnavos Basin, Greece. J Geodyn 36:19–35. doi:10.1016/S0264-3707(03)00036-X

Carvalho J, Cabral J, Gonçalves R, Torres L, Mendes-Victor L (2006) Geophysical methods applied to fault characterization and earthquake potential assessment in the Lower Tagus Valley, Portugal. Tectonophysics 418:277–297. doi:10.1016/j.tecto.2006.02.010

Cottes L (1924) Le lac d'Oisans. Bulletin de la Société Dauphinoise d'Ethnographie et d'Archéologie, pp 62–78

Cushing EM, Bellier O, Nechtschein S, Sébrier M, Lomax A, Volant P, Dervin P, Guignard P, Bove L (2007) A multidisciplinary study of a slow-slipping fault for seismic hazard assessment: the example of Middle Durance Fault (SE France). Geophys J Int (in press)

Delgado J, Lopez Casado C, Estevez AC, Giner J, Cuenca A, Molina S (2000) Mapping soft soils in the Segura river valley (SE Spain): a case study of microtremors as an exploration tool. J Appl Geophys 45:19–32. doi:10.1016/S0926-9851(00)00016-1

Demanet D, Renardy F, Vanneste K, Jongmans D, Camelbeeck T, Megrahoui M (2001) The use of geophysical prospecting for imaging active faults In the Roer Graben, Belgium. Geophysics 66:78–89. doi:10.1190/1.1444925

Dix CH (1955) Seismic velocities from surface measurement. Geophysics 20:68–86. doi:10.1190/1.1438126

Fernandez A, Guillot S, Menot RP, Ledru P (2002) Late Paleozoic polyphased tectonics in the SW Belledonne massif (External Crystalline Massifs, French Alps). Geodin Acta 15:127–139. doi:10.1016/S0985-3111(02)01084-7

Gamond JF (1994) Normal faulting and tectonic inversion driven by gravity in a thrusting regime. J Struct Geol 16:1–9. doi:10.1016/0191-8141(94)90013-2

Goffé B, Schwartz S, Lardeaux JM, Bousquet R (2004) Exploratory notes to the map: metamorphic structure of the Alps, Western and Ligurian Alps. Mitt Osterereichischen Mineralogischen Ges 149:125–144

Gratier JP, Ménard G, Arpin R (1989) Strain-displacement compatibility and restoration of the Chaînes Subalpine of the western Alps. Geol Soc Spec Publ 45:65–81

Green A, Gross R, Holliger K, Horstmeyer H, Baldwin J (2003) Results of 3-D georadar surveying and trenching the San Andreas fault near its northern landward limit. Tectonophysics 368:7–23. doi:10.1016/S0040-1951(03)00147-1

Guéguen P, Cornou C, Garambois S, Banton J (2007) On the limitation of the *H/V* spectral ratio using seismic noise as an exploration tool: application to the Grenoble Valley (France), a small apex ratio basin. Pure Appl Geophys 164:115–134. doi:10.1007/s00024-006-0151-x

Guillier B, Cornou C, Krister J, Moczo P, Bonnefoy-Claudet S, Bard PY, Fäh D (2006) Simulation of seismic ambient vibrations: does the *H/V* provide quantitative information in 2D-3D structures? Third international symposium on the effects of surface geology on seismic motion Grenoble, France, 30 August–1 September 2006 Paper Number 185

Guillot S, Ménot RP (1999) Nappe stacking and late Variscan extension in the Belledonne Massif (ECM, French Alps). Geodin Acta 12:97–111. doi:10.1016/S0985-3111(99)80026-6

Jongmans D, Pitilakis K, Demanet D, Raptakis D, Riepl J, Horrent C, Tsokas G, Lontzetidis K, Bard PY (1998) EURO-SEISTEST: determination of the geological structure of the Volvi basin and validation of the basin response. Bull Seismol Soc Am 88:473–487

Koller MG, Chatelain JL, Guillier B, Duval AM, Atakan K, Lacave C, Bard PY (2004) Practical user guidelines and software for the implementation of the *H/V* ratio technique: measuring conditions, processing method and results interpretation. Proceedings of the 13th world conference in earthquake engineering, Vancouver, August 2004, Paper 3132

Konno K, Ohmachi T (1998) Ground motion characteristics estimated from spectral ratio between horizontal and vertical components of microtremor. Bull Seismol Soc Am 88(1):228–241

Loke MH (1998) Res2dInv, rapid 2D resistivity and IP inversion using the least squares method—user's manual

Loke MH, Barker RD (1996) Least-squares deconvolution of apparent resistivity pseudosections. Geophysics 60(6):1682–1690. doi:10.1190/1.1443900

Martinod J, Jouanne F, Taverna J, Ménard G, Gamond JF, Darmendrail X, Notter JC, Basile C (1996) Present-day deformation of the Dauphiné (SE France) Alpine and Subalpine massifs. Geophys J Int 127:189–200. doi:10.1111/j.1365-246X.1996.tb01544.x

Martinod J, Roux L, Gamond JF, Glot JP (2001) Present-day deformation of the Belledonne Massif (External Alps, France): comparison triangulation-GPS. Bull Soc Geol Fr 172:713–721. doi:10.2113/172.6.713

MacGregor KR, Anderson RS, Anderson SP, Waddington ED (2000) Numerical simulations of glacial-valley longitudinal profile evolution. Geology 28(11):1031–1034. doi:10.1130/0091-7613(2000)28<1031:NSOGLP>2.0.CO;2

Ménot RP (1988) An overview of the geology of the Belledonne massif (external crystalline massifs of Western Alps). Schweiz Mineral Petrogr Mitt 70:33–53

Meric O, Garambois S, Jongmans D, Wathelet M, Chatelain JL, Vengeon JM (2005) Application of geophysical methods for the investigation of the large gravitational mass movement of Séchilienne. France Can Geotech J 42:1105–1115. doi:10.1139/t05-034

Molnar P, Anderson RS, Anderson SP (2007) Tectonics, fracturing of rock, and erosion. J Geophys Res 112:F03014. doi:10.1029/2005JF000433

Montjuvent G, Winistorfer J (1980) Glaciations quaternaires dans les Alpes franco-suisses et leur piedmont. Geologie Alp 56:251–282

Nakamura Y (1989) A method for dynamic characteristics estimation of subsurface using microtremor on the ground surface. Q Rep Railway Tech Res Inst 30(1):25–30

Nogoshi M, Igarashi T (1972) On the amplitude characteristics of microtremor (Part 2) (in Japanese with English abstract). J Seismol Soc Jpn 24:26–40

Nguyen F, Garambois S, Chardon D, Hermitte D, Bellier O, Jongmans D (2007) Subsurface electrical imaging of anisotropic formations affected by a slow active reverse fault, Provence, France. J Appl Geophys (in press)

Parolai S, Bormann P, Milkert C (2002) New relationships between *Vs*, thickness of sediments, and resonance frequency calculated by the *H/V* ratio of seismic noise for Cologne Area (Germany). Bull Seismol Soc Am 92:2521–2527. doi:10.1785/0120010248

Pothérat P, Alfonsi P (2001) Les mouvements de versant de Séchilienne (Isère). Prise en compte de l'héritage structural pour leur simulation numérique. Rev Fr Geotechniq 95(96):117–131

Shields G, Allander K, Brigham R, Crosbie R, Trimble L, Sleeman M, Tucker R, Zhan H, Louie JN (1997) Shallow Geophysical Survey across the Pahrump Valley Fault Zone, California–Nevada Border. Bull Seismol Soc Am 88(1):270–275

Siame L, Bellier O, Braucher R, Sébrier M, Cushing M, Bourlès D, Hamelin B, Baroux E, de Voogd B, Raisbeck G, Yiou F (2004) Local erotion Rates versus active tectonics: cosmics ray exposure modelling in Provence (South-East France). Earth Planet Sci Lett 220(3–4):345–364. doi:10.1016/S0012-821X(04)00061-5

Spear FS (1993) Metamorphic Phase Equilibria and Pressure-Temperature-Time Paths. Mineralogical Society of America, Monograph series, 799p

Stephenson WJ, Odum JK, Williams RA, Anderson ML (2002) Delineation of faulting and basin geometry along a seismic reflection transect in urbanized San Bernardino Valley, California. Bull Seismol Soc Am 92:2504–2520. doi:10.1785/0120010222

Suzuki K, Toda S, Kusunoki K, Fujimitsu Y, Mogi T, Jomori A (2000) Case studies of electrical and electromagnetic methods applied to mapping active faults beneath the thick. Quaternary Eng Geol 56:29–45. doi:10.1016/S0013-7952(99)00132-5

Telford WM, Geldart LP, Sheriff RE (1990) Applied geophysics, 2nd edn. Cambridge University Press, Cambridge, p 751

Thouvenot F, Frechet J, Jenatton L, Gamond JF (2003) The Belledonne Border Fault: identification of an active seismic strike-slip fault in the western Alps. Geophys J Int 155:174–192. doi:10.1046/j.1365-246X.2003.02033.x

Tokimatsu K (1997) Geotechnical site characterization using surface waves. In: Ishihara K (ed) Proc. 1st intl. conf. earthquake geotechnical engineering, vol 3, pp 1333–1368

Uebayashi H (2003) Extrapolation of irregular subsurface structures using the horizontal to vertical spectra ratio of long period microtremors. Bull Seismol Soc Am 93(2):570–582. doi:10.1785/0120020137

Van der Beek P, Bourbon P (2008) A quantification of the glacial imprint on relief development in the French western Alps. Geomorphology (in press)

Vengeon JM, Giraud A, Antoine P, Rochet L (1999) Analysis of the deformation and toppling of rock slopes in crystallophyllian terrain. Can Geotech J 36:1123–1136. doi:10.1139/cgj-36-6-1123

von Raumer JF, Ménot RP, Abrecht J, Biino G (1993) The pre-Alpine evolution of the external massifs. In: von Raumer J, Neubauer F (eds) The pre-Mesozoic geology in the Alps. Springer, Berlin, pp 221–240

Wathelet M (2003) Report on the inversion of velocity profile and version 0 of the inversion software. SESAME report D14.07

Wells DL, Coppersmith J (1994) New empirical relationships among magnitude, rupture length, rupture width, rupture area, and surface displacement. Bull Seismol Soc Am 84:974–1002

Whiteley RJ, Hunter JA, Pullan S (1986) High-resolution common-offset seismic reflection profiling in the Chaophraya basin, Bangkok, Thailand. SEG Technical Program Expanded Abstracts 104–106